RL-TR-91-88
In-House Report
April 1991

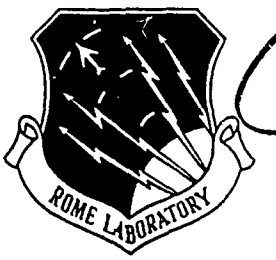

MATERIAL EFFECTS IN PHOTOCONDUCTIVE FROZEN WAVE GENERATORS

Robert M. O'Connell; J.B. Thaxter; Richard E. Bell, Capt, USAF

APPROVED FOR PUBLIC RELEASE; DISTRIBUTION UNLIMITED.

Rome Laboratory
Air Force Systems Command
Griffiss Air Force Base, NY 13441-5700

This report has been reviewed by the Rome Laboratory Public Affairs Division (PA) and is releasable to the National Technical Information Service (NTIS). At NTIS it will be releasable to the general public, including foreign nations.

RL-TR-91-88 has been reviewed and is approved for publication.

APPROVED:

ROBERT J. MAILLOUX
Chief, Antennas & Components Division
Directorate of Electromagnetics

APPROVED:

JOHN K. SCHINDLER
Director of Electromagnetics

FOR THE COMMANDER:

JAMES W. HYDE III
Directorate of Plans & Programs

If your address has changed or if you wish to be removed from the Rome Laboratory mailing list, or if the addressee is no longer employed by your organization, please notify Rome Laboratory (EEAC) Hanscom AFB MA 01731-5000. This will assist us in maintaining a current mailing list.

Do not return copies of this report unless contractual obligations or notices on a specific document require that it be returned.

REPORT DOCUMENTATION PAGE

Form Approved
OMB No 0704-0188

1. AGENCY USE ONLY (Leave blank)	2. REPORT DATE	3 REPORT TYPE AND DATES COVERED
	April 1991	In-House, 1 JUN 89 - 30 SEP 89

4 TITLE AND SUBTITLE
Material Effects in Photoconductive Frozen Wave Generators

5 FUNDING NUMBERS
PE: 62702F
PR: 2305
TA: J5
WU: 05

6. AUTHOR(S)
* Robert M. O'Connell
J. Bruce Thaxter
Richard, E. Bell, Capt. USAF

7. PERFORMING ORGANIZATION NAME(S) AND ADDRESS(ES)
Rome Laboratory/EEAC
Hanscom AFB, MA 01731

8. PERFORMING ORGANIZATION REPORT NUMBER
RL-TR-91-88

9 SPONSORING/MONITORING AGENCY NAME(S) AND ADDRESS(ES)

10. SPONSORING/MONITORING AGENCY REPORT NUMBER

11 SUPPLEMENTARY NOTES
* Robert M. O'Connell - Participated in this work under the 1989 USAF-UES Summer Faculty Research Program sponsored by the Air Force Office of Scientific Research.

12a DISTRIBUTION/AVAILABILITY STATEMENT
Approved for public release; distribution unlimited.

12b. DISTRIBUTION CODE

13 ABSTRACT (Maximum 200 words)

Linear photo-conductive gallium arsenide (GaAs) fast closing switches for microwave applications, such as frozen wave pulse generation, are analyzed and compared to experimental measurements. Material effects in photo-conductive frozen wave generators fabricated in semiconductor-based microstrip transmission line are studied from three perspectives; frozen wave propagation in the line; the spacing between the switches in a frozen wave generator and their maximum number; and the switching behavior of the gap-switch itself, which is modeled as a lumped-element, modified Ebers-Moll equivalent circuit. The experimental transient behavior of hybrid gap-switches fabricated on semi-insulating GaAs with ohmic and non-ohmic contacts is compared with predicted performance. Picosecond laser pulses, doubled to 527 μm wavelength are used to excite linear photoconductivity in 75 μm gap switches mounted in a test fixture of 50 ohm microstrip lines on alumina.

14 SUBJECT TERMS
Frozen waves, Photonic, Short-pulse microwaves, Laser activated photoconductive switches

15 NUMBER OF PAGES
36

16 PRICE CODE

17 SECURITY CLASSIFICATION OF REPORT	18 SECURITY CLASSIFICATION OF THIS PAGE	19 SECURITY CLASSIFICATION OF ABSTRACT	20 LIMITATION OF ABSTRACT
Unclassified	Unclassified	Unclassified	SAR

NSN 7540-01-280-5500

Standard Form 298 (rev 2-89)
Prescribed by ANSI Std Z39-18
298-102

Contents

Illustrations

Material Effects in Photoconductive Frozen Wave Generators

1. INTRODUCTION

This work is motivated by the promise of frozen wave generators (FWG) to provide high power, wide band, pulsed microwave signal sources at very low cost. The technique is amenable to monolithic fabrication, especially at higher microwave frequencies, thus allowing fabrication of phased arrays with large numbers of elements for specialized Air Force radar and communications applications. Using basic frozen wave concepts, outlined below, static electric energy stored at the array radiating aperture in simple microwave circuit elements is released in the form of a microwave pulse via photonically controlled photoconductive switches. Since this pulse is generated essentially at the radiator, the usual problems of signal dispersion and loss in the microwave feed structures are avoided. The peak pulse power radiated from the array elements combine in space forming beams useful for very wide band radar and communication systems.

These future Air Force system requirements include the need for low-cost, lightweight sources of pulsed microwave energy. A typical pulse is illustrated in Figure 1 along with its amplitude spectrum[1]. Note that the center frequency f_0 of the microwave pulse is determined

(Received for Publication 1 May 1991)

[1] Haykin, Simon (1983) *Communication Systems, 2nd Ed.*, New York, NY, John Wiley and Sons, p. 20.

by the period T of a single cycle of the microwave signal within the pulse and that the amount of energy in the main lobe and its spread Δf (the bandwidth) about f_0 are determined by the temporal width P of the microwave pulse.

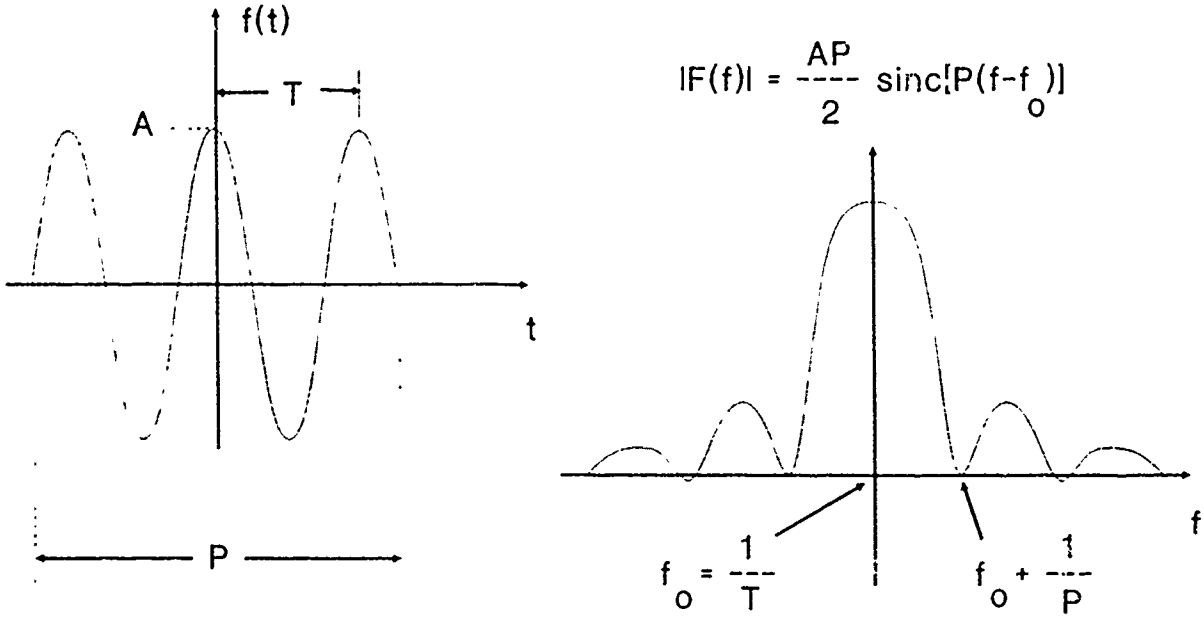

Figure 1. A Typical RF or Microwave Pulse f(t) and its Amplitude Spectrum F(f).

The signal of Figure 1 is closely approximated by the pulse train shown in Figure 2, which can in principle be produced very simply with a FWG[2,3] such as that illustrated in Figure 3. If the switches of the FWG are closed simultaneously and very quickly while the transmission line segment between them is charged to +V volts, the wave shown in the figure will be launched. This happens because one half of the energy stored on the charged (+V) line segment travels to the right and the other half travels to the left. This latter half reflects and reverses phase at the short circuit, then travels back through both switches (assuming they are still closed) to follow the first half of the signal and form the single cycle waveform shown in Figure 3. More cycles can be added to the wave by using more switches and alternating the polarity of the voltage (±V) on the line segments between successive pairs of switches. Note that half of the period of the wave is determined by the length of line X between the switches and the phase velocity v_p of the wave on the line through the relation

2 Proud, J.M. and Norman, S.L. (1978) High frequency waveform generation using optoelectronic switching in silicon. *IEEE Trans. Microwave Theory Tech.*, **MTT-26**:137.

3 Lee, C.H., Li, M.G., Chang, C.S., Yurek, A.M., Rhee, M.J., Chauchard, E., Fischer, R.P., Rosen, A., and Davis, H. (1985) Optoelectronic techniques for microwave and millimeter-wave applications. *Proc. IEEE MTT S International Microwave Symposium*, St. Louis, MO, p. 178.

$$V_p T/2 = X. \quad (1)$$

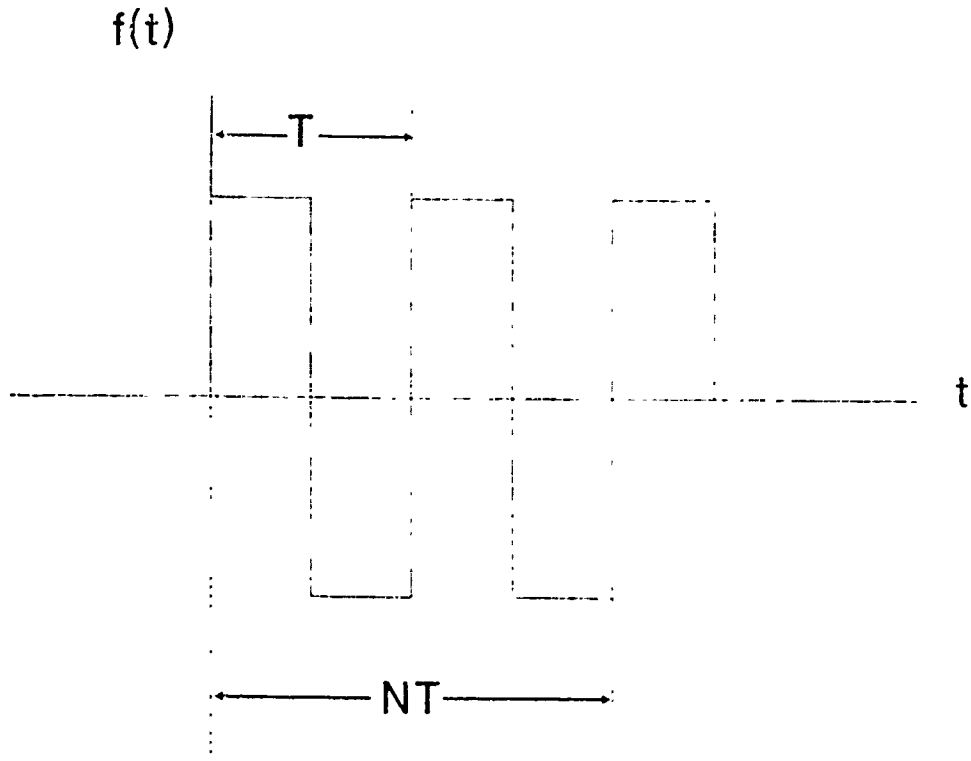

Figure 2. A Pulse Train That Closely Approximates the Signal of Figure 1.

We are developing circuits to produce microwave frozen waves at gigahertz frequencies as illustrated in Figure 3 by using short photoconductive gaps as switches in microstrip transmission lines. Since the center frequency of the microwave pulse equals 1/T (this is only approximately true, as we'll see later), gigahertz signals will have nanosecond periods and the switches must close in times much shorter than a period. Consequently, the effort is aimed at using state-of-the-art picosecond laser pulses to close the switches by drastically changing the electrical conductivity of the material in the switch (the gap in the microstrip) from very low to very high (through the photoconductive effect). An obvious choice of material for this is a semi-insulating semiconductor. Thus, the overall approach to the project is to produce frozen waves using photoconductive switches (gaps) in semiconductor-based microstrip switch chips in a hybrid circuit having charged transmission line segments of 50 ohm microstrip on

alumina substrates. The new device being added to the traditional frozen wave technology is the high power picosecond laser capable of delivering multiple beams of precisely timed pulse trains. These extremely fast rise-time coherent optical pulses can accurately trigger the PC switches well within a small fraction of a period of the desired microwave frequency.

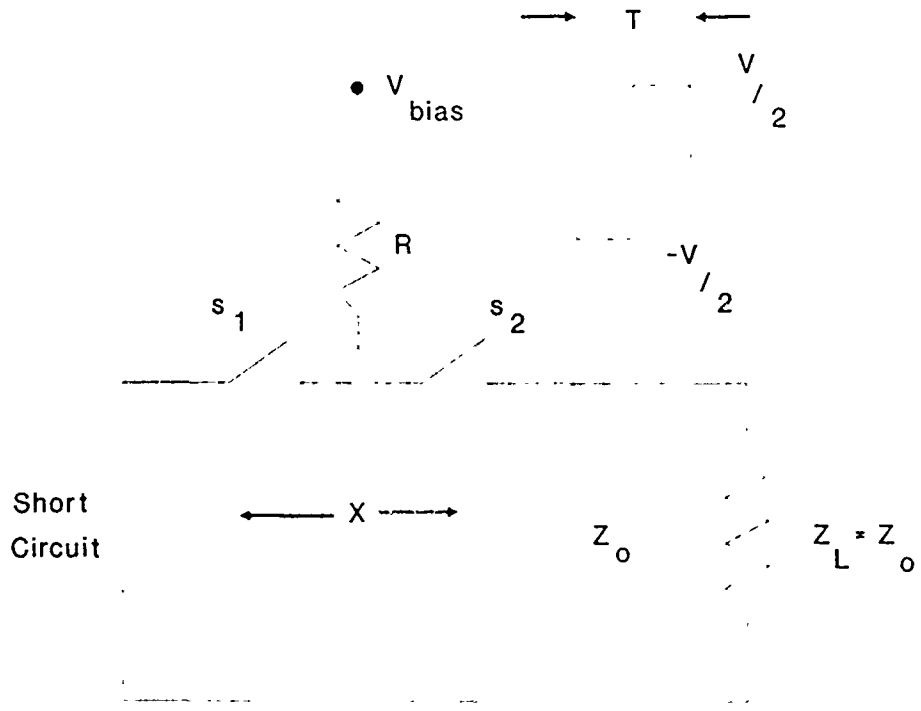

Figure 3. A One-cycle Frozen Wave Generator Consisting of Two Switches S_1 and S_2 Embedded in a Transmission Line That is Short Circuited at S_1 and Terminated in a Matched Load.

This report is limited to the analysis and preliminary experimental observations of a few gap-switches made during a 10 week UES-SVRF Program of one of the authors, RMO.

2. OBJECTIVES OF THE RESEARCH EFFORT

At the outset of the project, it was presumed that the frozen wave generators to be built and tested would consist of short gaps in the upper conductors of microstrip transmission lines based on semi-insulating semiconductors. Thus, the material properties of the semiconductor will affect both the behavior of the switch (speed, resistance, etc.) and the propagation characteristic (impedance, etc.). Accordingly, a major goal of the project is to seek optimum materials for the frozen wave generators.

To make wise decisions concerning materials, it is necessary to thoroughly understand the behavior of the frozen wave generator and, even more importantly, the basic photoconductive switch. Thus, as the project progressed, three important objectives evolved, which are essential for the successful fabrication of a FWG.

1. Investigate how material properties affect the propagation of a frozen wave traveling in microstrip.

2. Investigate how material properties affect the spacing and number of switches in the frozen wave generator.

3. Investigate how material properties affect the behavior of the photoconductive switches themselves.

In the next section, the approaches taken toward achieving these objectives and the results obtained will be described and discussed.

3. APPROACHES AND RESULTS

3.1 Material Effects on Frozen Wave Propagation in Microstrip

The important materials-related properties of microstrip transmission line, a cross-section of which is illustrated in Figure 4, are its characteristic impedance Z_0, effective relative dielectric constant ε_{re}, dielectric attenuation constant α_d, and strip conductor attenuation constant loss α_c. Z_0 is important for impedance matching and α_d and α_c are important for loss considerations. The importance of ε_{re} will be discussed in the next section.

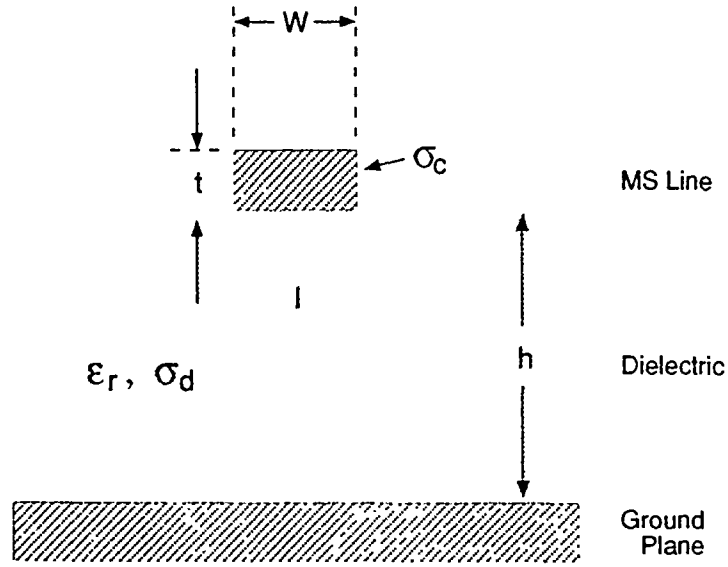

Figure 4. Microstrip (MS) Cross-Section, Illustrating the Width w and Thickness t of the Upper Strip Conductor and the Dielectric or Semiconductor Substrate Thickness h. ε_r is the relative dielectric constant of the substrate and α_c and α_d are the electrical conductivities of the strip conductor and substrate, respectively.

Highly accurate approximate analyses of the structure in Figure 4 have been performed and complete tabulations of the rather cumbersome results are widely available.[4,5] For our purposes, it is only necessary to indicate the functional dependences of Z_0, ε_{re}, α_d, and α_c, which are as follows:

$$Z_0 = Z_0 (\varepsilon_r, f, w/h, t/h, h), \tag{2a}$$

$$\varepsilon_{re} = \varepsilon_{re} (\varepsilon_r, f, w/h, t/h, h), \tag{2b}$$

$$\alpha_d = \alpha_d(\varepsilon_r, \sigma_d, w/h, t/h), \tag{2c}$$

$$\alpha_c = \alpha_c (\varepsilon_r, \sigma_c, w/h, t/h), \tag{2d}$$

---

[4] Gupta, K.C., Garg, R., and Bahl, I.J. (1979) *Microstrip Lines and Slotlines*. Dedham, MA Artech House, p. 88.

[5] Bahl, I.J. and Bhartia, P. (1980) *Microstrip Antennas*, Dedham, MA. Artech House, p. 309.

where f refers to frequency and the other quantities in the parentheses are defined in Figure 4. Thus, for a given material system, there is a rather complicated interrelationship among frequency, waveguide geometry, and the material properties (ε_r, σ_d, and σ_c), which must be considered. This can be done using commercially available software,[6] in which the equations suggested by Eqs. (2a)-(2d) are programmed.

3.2 Material Effects on the Spacing and Number of Switches in the Frozen Wave Generator

The elementary concept that the product of velocity and time equals distance leads to the equation

$$X = V_p T/2. \tag{1}$$

as stated in the Introduction. It relates the period T of one cycle of a frozen wave pulse train to the phase velocity, V_p, of the wave on a transmission line and the spacing X of the switches that comprise the frozen wave generator. Since, in microstrip,[5]

$$V_p = c/\sqrt{\varepsilon_{re}} \tag{2}$$

where c = the free space speed of light. Eq. (1) can be rewritten

$$X = cT/2\sqrt{\varepsilon_{re}}. \tag{3}$$

As promised in the last section, this equation shows the importance of the effective relative dielectric constant ε_{re} in device design. Also, since ε_{re} depends on the relative dielectric constant ε_r of the substrate (as stated in functional Eq. (2b)), it follows that Eq. (3) also shows that the substrate material affects the switch spacing. The exact behavior of this dependence would require the use of the exact equation represented by Eq. (2b) in Eq. (3).

To appreciate the relationship between material properties and the number of switches in the generator, it is necessary to consider the amplitude spectrum of the frozen wave. (The

[6] SUPERCOMPACT, for example, is one such software package.

number of switches is one more than the number of cycles in the frozen wave.) As illustrated in Figure 1, if the frozen wave were a truly sinusoidal pulse train, the relation

$$f_0 = 1/T \tag{4}$$

would be exactly correct and Eq. (3) could be rewritten in the convenient form

$$X = c/2\sqrt{\varepsilon_{re}}\, f_0. \tag{5}$$

Furthermore, as is also illustrated in Figure 1, as the width P of the pulse train increases, its energy becomes concentrated in an increasingly narrower band of frequencies Δf centered on f_0. If these results were also exactly true of the frozen wave shown in Figure 2, it would follow that the number of cycles N in the frozen wave would only affect the bandwidth of the signal, that is, by associating NT with P (see in Figures 1 and 2) the bandwidth would decrease with increasing N. As we will show, however, N also affects the center frequency of the square wave pulse train, so that Eq. (4) must be replaced by a functional equation of the form

$$f_0 = f_0\,(N,\, 1/T). \tag{6}$$

Using this form, Eq. (5) should also be rewritten as

$$X = c/\sqrt{\varepsilon_{re}}\, f_0\,(N,\, 1/T). \tag{7}$$

If f(t) and $f_1(t)$ represent the signal in Figure 2 and one of its cycles, respectively, f(t) can be expressed as

$$f(t) = \sum_{n=1}^{N} f_1\,[t - (n-1)]\,T. \tag{8}$$

By the Shifting Theorem of spectral analysis, the Fourier transform [F(ω)] of f (t) can be written as

$$F(\omega) = F_1(\omega) \sum_{n=1}^{N} e^{-j\omega(n-1)T} \tag{9}$$

where $F_1(\omega)$ is the transform of $f_1(t)$. It is straightforward to show that

$$F_1(\omega) = \frac{A}{j\omega}\left(1 - e^{-j\omega T/2}\right)^2 = jAT\, e^{-j\omega T/2} \cdot \frac{\sin^2 \omega T/4}{\omega T/4}. \tag{10}$$

Also, using information in Reference 7, we can write

$$\sum_{n=1}^{N} e^{-j\omega(n-1)T} = \sum_{n=0}^{N-1} e^{-j\omega nT} = \frac{1 - e^{-j\omega NT}}{1 - e^{-j\omega T}} \tag{11}$$

$$= e^{j\omega T(n-1)/2}\, \frac{\sin(\omega NT/2)}{\sin(\omega T2)}.$$

Finally, using Eqs. (10) and (11), we can express the amplitude spectrum $|F(\omega)|$ as

$$|F(\omega)| = AT \left| \frac{\sin^2(\omega T/4)}{\omega T/4} \cdot \frac{\sin(\omega NT/2)}{\sin(\omega T/2)} \right|. \tag{12}$$

Plots of this equation would show that the main lobe of $|F(\omega)|$ is centered on a frequency f_0 that is somewhat to the left of 1/T and approaches 1/T with increasing N. Furthermore, $|F(\omega)|$ becomes more symmetrical about f_0 with increasing N with a bandwidth proportional to 1/N. Thus, the behavior of $|F(\omega)|$ for the square wave pulse train is similar to that of the sinusoidal pulse train when N is large.

To briefly illustrate these points, note that for N = 1 the second factor of Eq. (10) is 1 and the first factor plots as shown in Figure 5. Differentiation of the first factor in Eq. (10) to determine the frequency of the main lobe results in the transcendental equation

$$\tan \omega T/4 = 2\, \omega T/4, \tag{13}$$

which can be solved iteratively to give

$$f_0 = 0.7417/T. \tag{14}$$

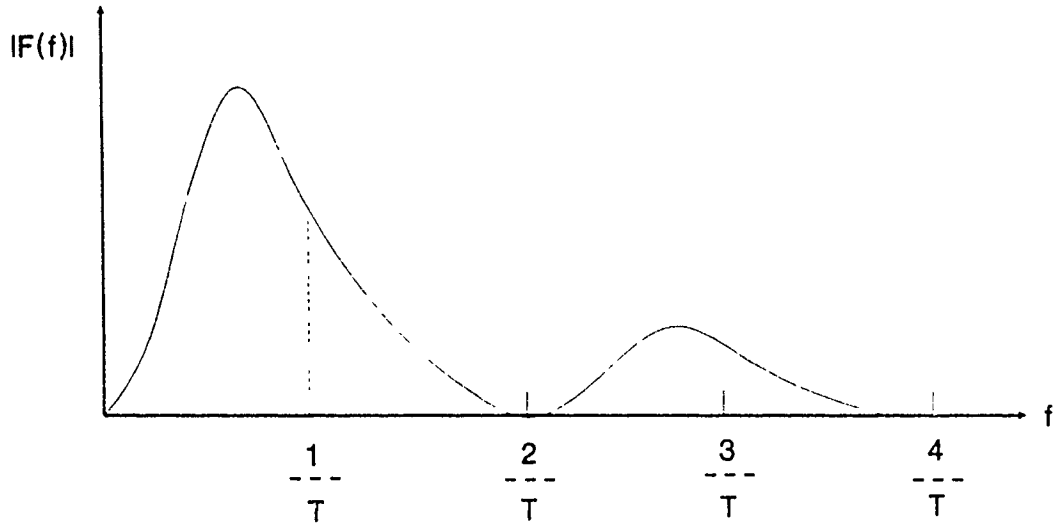

Figure 5. Plot of Eq. (10) for N = 1, which is also the First Factor in Eq. (10).

For N > 1, the plot of Figure 5 must be multiplied by the second factor in Eq. (10) Plots of this factor for N = 2 and 3 are shown in Figure 6. It is apparent that the product of the curve in Figure 5 with each of these curves will have a peak frequency that approaches 1/T as N gets larger. Also, the resultant spectrum becomes more symmetrical about f_0 with increasing N and has a bandwidth proportional to 1/N. We have now shown how both the center frequency f_0 and the bandwidth Δf of the square pulse train form of frozen wave depend on the number N of cycles in the frozen wave or, equivalently, on the number (N + 1) of switches in the frozen wave generator.

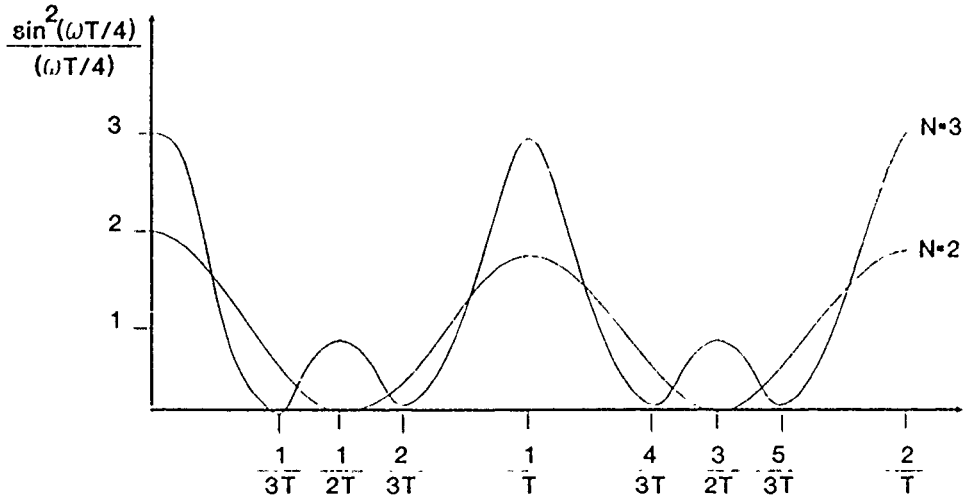

Figure 6. Plots of the Second Factor in Eq. (10) for N = 2 and 3.

3.3 Material Effects on Photoconductive Switches

Having considered the transmission medium and the number and spacing of switches in a frozen wave generator, we now consider the behavior of the photoconductive switches themselves. As discussed in the introduction and illustrated with the help of Figure 3, for the frozen wave to form properly, all (N + 1) switches in the generator have to remain closed while all of the segments of the wave work their way to the left and right, and ultimately leave the generator, traveling to the right. If N is large, which would be desirable if a narrow-band, high-power signal were required, this could require a fairly long switch closure time. Since the switches are to be made of an illuminated semiconductor, this means that the recombination lifetime τ of the substrate material has to be sufficiently long. Thus, in this manner, the recombination lifetime of the substrate material limits the number of switches in the frozen wave generator. Furthermore, since the frequency f_0 of the main lobe of the signal spectrum varies with N as discussed above, τ affects f_0 as well as Δf. The results of the present section should make it possible to, among other things, decide how many switches can be used in a given generator using a given material system.

Our approach to studying a single photoconductive switch is to model it for use in the well-known SPICE simulation program. An appropriate switch model includes both material and device parameters for the switch. Such a model, embedded between segments of transmission line, is analyzed with SPICE. The analysis would include the full range of device behavior from the unilluminated OFF state through the transient leading to the illuminated ON state and finally through the transient leading back to the OFF state.

The first decision to be made is whether the switch model is to be composed of lumped rather than distributed elements. Since the length of a typical switch (the size of the gap in

the strip conductor of the microstrip line) is of the order of (at most) tens of microns, and since the wavelength of a gigahertz signal in typical microstrip is of the order of centimeters, a lumped-element model is appropriate for the present work. However, when higher frequencies (the millimeter-wave regime) are considered, the lumped-element model will have to be revised.

To illustrate some of the logic that led to the lumped-element switch model, Figure 7 shows a cross-section of a typical photoconductive switch (the gap) in microstrip. Note first that there is clearly a capacitance C_g, between the electrodes on either side of the gap. Secondly, when the gap is illuminated, the increased conductivity of the semiconductor will allow (and control) an electrical current between A and B. Thus, there is also a light-controlled variable resistor between the electrodes. Finally, because the substrate is semi-insulating, the metal-semiconductor contacts where the strip electrode meets the substrate at the edges of the gap are probably significantly non-ohmic,[8] that is, they probably form Schottky diodes. We observed such non-ohmic behavior in a preliminary measurement on a photoconductive switch, as described more fully in Section 3.4 below.

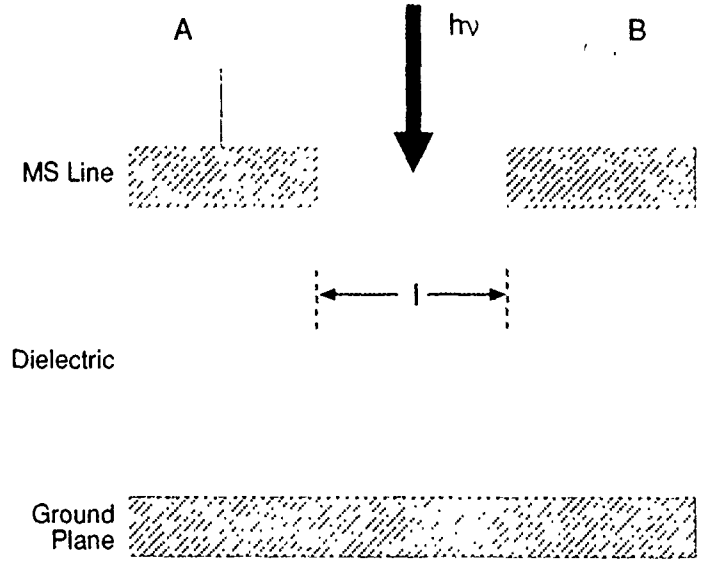

Figure 7. Cross Section of an Illuminated Photoconductive Switch in Microstrip. l is the length of the gap in the strip conductor.

When the unbiased gap is illuminated with a laser pulse, a negative electrical pulse was observed on the oscilloscope. This signal can be explained if there is a rectifying contact between electrode A and the substrate, electrons produced by the absorbed photons thus see a

[8] Auston, D.H. Chapter 4 in Lee, C.H., ed., (1984) *Picosecond Optoelectric Devices*, New York, NY, Academic Press.

downhill potential and generate the observed signal via the photovoltaic effect.[9] Incidentally, when terminal B was terminated in either a short or an open, the oscilloscope signal was modified by the reflected signals as would be expected.

The preceding ideas suggest that the switch be modeled as a phototransistor with a variable resistor between the junctions and a shunt capacitor, as shown in Figure 8. The shunt capacitor C_g has been analyzed by Maeda[9] and is a function of the static relative dielectric constant, ε_r, of the semiconductor, as well as geometric factors. Values of 20-50 fF are typical. The junctions are modeled using a symmetric Ebers-Moll model[10] to allow any bias (forward and reverse) across each junction. Capacitances associated with the junction should automatically be accounted for by the SPICE program. Note that if the junctions are non-rectifying, the diodes become short circuits and the model becomes a parallel resistor/capacitor combination, as discussed by Auston.[8]

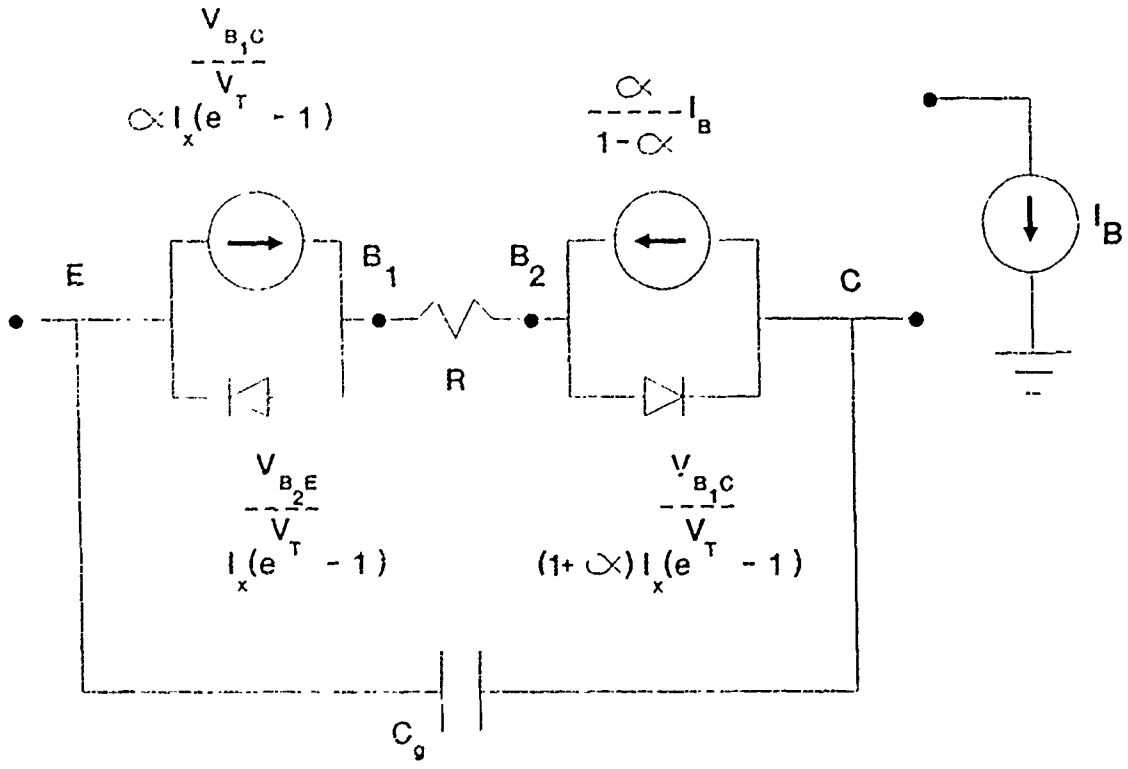

Figure 8. Lumped-element Model of the Photoconductive Switch.

[9] Maeda, M. (1972) An analysis of gap in microstrip transmission lines. *IEE Trans. Microwave Theory Tech.*, **MTT-20**:390.

[10] Muller, R.S. and Kamnis, T.I. (1981) *Device Electronics for Integrated Circuits, 2nd Ed.*, New York, NY, John Wiley and Sons, p. 294.

The Ebers-Moll model introduces the parameters α and I_x. These parameters are somewhat complicated functions of both geometry and material properties, including the lifetimes and mobilities of charge carriers and the band gap (or intrinsic density) of the semiconductor. Exact functional forms for these parameters remain to be established.

The remaining parameters in the model, I_B and R, are functions of the time varying optical power in the pulsed laser that is used to close the switch. I_B is the light-induced photocurrent, which can be expressed as[11]

$$I_B = \frac{e\eta\,(1-r)\,P\,(t)}{h\upsilon} \tag{15}$$

where e is the electron charge, r is the reflectivity of the semiconductor at the wavelength of the light pulse, $h\upsilon$ is the photon energy in the beam, P(t) is the optical power that reaches the semiconductor, and η is the quantum efficiency for conversion of photons to electron-hole pairs. Both η and r are material properties.

An expression for R can be developed[12] by approximating the illuminated volume between terminals A and B in Figure 7 as a parallelpiped as illustrated in Figure 9. The dimensions, l, w, and d represent, respectively, the length of the gap (see Figure 7), the width of the strip conductor (see Figure 4), and an effective or average absorption depth of the light. The depth d is often approximated by $1/\beta$, where β is the absorption coefficient of the material at the laser wavelength.[11]

[11] Sze, S.M. (1981) *Physics of Semiconductor Devices, 2nd Ed.*, New York, NY, John Wiley and Sons, p. 745.

[12] Nunnaly, W.C. and Hammond, R.B. (1984) Chapter 12, in Lee, C.H., ed., *Picosecond Optoelectric Devices*, New York, NY Academic Press.

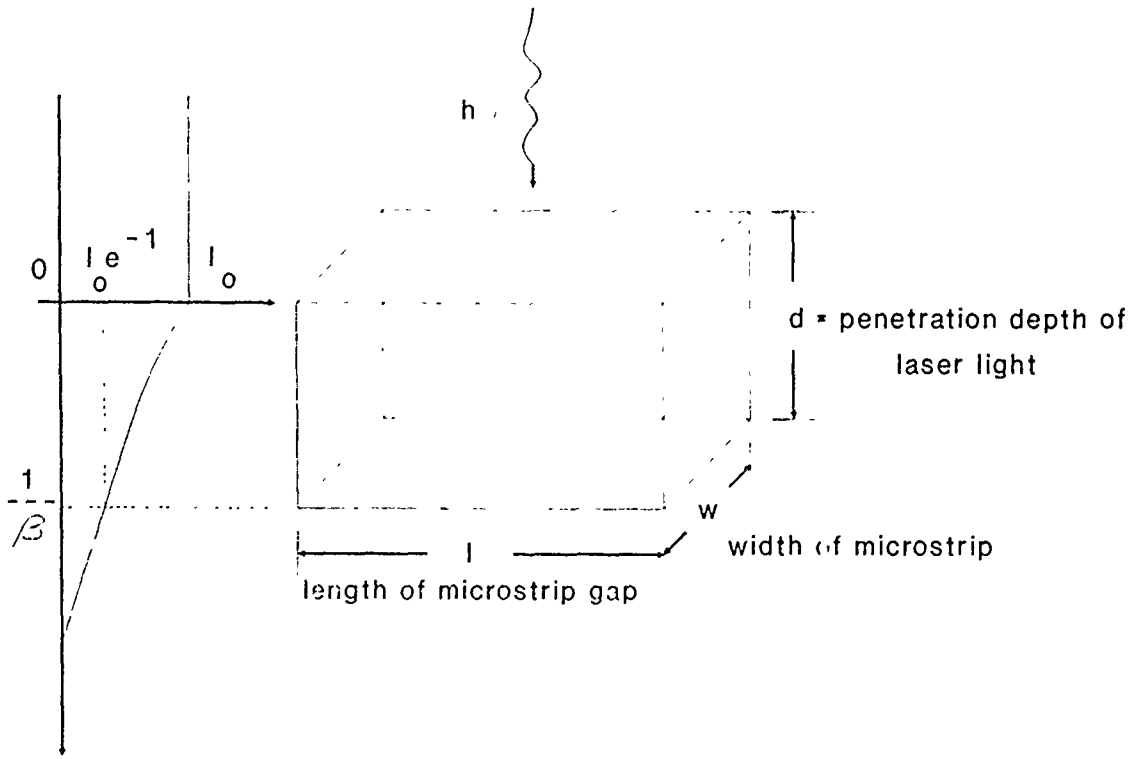

Figure 9. Geometry Used to Approximate the Illuminated Volume in a Photoconductive Switch. l = gap length, w = strip conductor width, d = effective absorption depth of the light.

The resistance R of the model in Figure 9 can be expressed as

$$R = l/\sigma(t)\, wd \tag{16}$$

where $\sigma(t)$ is the electrical conductivity of the material. Since the material is assumed to be semi-insulating, $\sigma(t)$ can be written as

$$\sigma(t) = e(\mu_n + \mu_p)\, n(t) \tag{17}$$

where μ_n and μ_p are the electron and hole mobilities, respectively, and n (t) is the concentration of free electron-hole pairs. n (t) can be written as the sum of intrinsic (n_i) and light-induced [Δn (t)] quantities as

$$n(t) = n_i + \Delta n(t), \tag{18}$$

so that Eq. (16) becomes

$$R = \frac{f}{wd\,e\left(\mu_n + \mu_p\right)\left[n_i + \Delta n(t)\right]}. \tag{19}$$

The change in the density of hole electron pairs may be modeled by the following differential equation used by Nunnaly and Hammond.[12]

$$\frac{d[\Delta n(t)]}{dt} = \frac{P(t)(1-r)}{h\mu wfd} - \frac{\Delta n(t)}{\tau} - \frac{(1-n_i)\,\Delta n(t)}{T_t}. \tag{20}$$

Let

$$\gamma = \frac{1}{\tau} + \frac{(1-n_i)}{t_t}. \tag{21}$$

and we have

$$\frac{d[\Delta n(t)]}{dt} + \gamma\,\Delta n(t) = \frac{P(t)(1-r)}{h\mu wfd}. \tag{22}$$

The above equation is a first order differential equation, the solution of which may be found in the first few chapters of a good differential equation text. In Eq. (20), τ is the recombination lifetime of Eq. (20) excess carriers in the material, η_i is the contact injection efficiency (a function of both the strip conductor and the semiconductor, which we have not

yet ascertained), and t_t is the transit time ($1/\mu_d$, where μ_d is the drift velocity, which depends on charge carrier mobilities).

Using the results of Reference 12, Δn (t) can be expressed as

$$\Delta n\,(t) = e^{-\gamma t}\int_0^t e^{\gamma t}\,\frac{\eta\,(1-r)\,P\,(t)\,d\,t}{h\,\mu w l\,d}\,. \tag{23}$$

If we define

$$F\,[P\,(t)] = e^{-\gamma t}\int_0^t e^{\gamma t}\,P\,(t)\,d\,t \tag{24}$$

for shorthand purposes, substitution of Eq. (23) into Eq. (19) yields

$$R\,(t) = \frac{}{ewd\,(\mu_n+\mu_p)}\;\frac{f}{\left\{n_i+\frac{\eta\,(1-r)}{h\,\mu w l d}\,F\,[P\,(t)]\right\}}\,. \tag{25}$$

It should be evident from the discussion in this section that the behavior of the photoconductive switch is a very complicated function of geometry and materials, including both the strip conductor (injection efficiency) and the semiconductor. The semiconductor properties that come into play are its relative dielectric constant ε_r, intrinsic density n_i or band gap E_g, lifetimes τ and mobilities μ of carriers, quantum efficiency η and absorption coefficient β, and reflectivity r. The easiest and most efficient way to consider the roles of these material parameters is to analyze different material/switch configurations using a simulation program such as SPICE.

Although the model presented here should be valid for analysis through the entire cycle of operation (from OFF to ON to OFF), some caution is needed in the ON state when the optical intensity is apt to be great enough to cause saturation or high-level injection effects. Where this happens, many of the material parameters very from their well-known "constant" value. For example, mobilities are known to drop significantly at high intensities.[13] Thus using the model correctly during the ON state will require a proper understanding of how the material properties behave under conditions of high level injection.

[13] Lee, C.H. (1984) Chapter 5 in Lee, C.H., ed., *Picosecond Optoelectric Devices*, New York, NY, Academic Press.

3.4 Experimental Results

3.4.1 FABRICATION

Ideally for FWG devices one wants a switch with zero "on" (closed) resistance, infinite "off" (open) resistance, zero rise time and no parasitics. The fall-time of the switch should be slow enough to pass the wave pulse but should recover high resistance to allow recharging the line segments. We selected 100 μm thick semi-insulating GaAs, a direct band gap semiconductor with a relatively high intrinsic resistivity and electron mobility as the substrate. Switches were configured as gaps in a 50 ohm microstrip transmission line to minimize parasitics and maximize wide band transient response. Four (4) 1 X 1 mm chips were designed, two with ohmic contacts, and two without. Switches were laid out in a pattern of four gaps per chip (see Figure 10) and the chips were hybrid bonded into a coplanar alumina waveguide with microwave fixtures for testing.

Non-ohmic contacts were formed automatically, due to the high resistivity of the GaAs substrate. Ohmic contacts were formed using ion implantation to make the material n^+ in the neighborhood of the upper microstrip conductor. The non-ohmic behavior of the switches fabricated without the ion-implantation step was observed by terminating one side of one such switch in 50 ohms and connecting the other side to a 50 ohm oscilloscope. When the unbiased gap was illuminated with a laser pulse, a negative electrical pulse was observed on the oscilloscope. The signal can be explained if there is a rectifying contact between the electrode and the substrate; electrons produced by the absorbed photons thus see a down-hill potential and generate the observed signal via the photovoltaic effect.[14] Incidentally, when the terminal was terminated in either a short or an open, the oscilloscope signal was modified as would be expected by the reflected signals.

3.4.2 DC CHARACTERISTICS

The DC "off" resistance and the average stand-off voltage of the four switch configurations were measured with a Tektronix Model 577/177 curve tracer. "Off" resistances were all over 10 Megohms. Also, it was determined that the switches could safely hold off a voltage of 2V per micron of gap width without damage to the switch or appreciable leakage currents. This is in line with other work and projects to a charged line potential of nominally 100V in the FWG or a peak RF power of approximately 100W.

---

[14] Bube, R.H. (1960) *Photoconductivity of Solids*, New York, NY, John Wiley and Sons, p. 78.

3.4.3 SWITCHING CHARACTERISTICS

Upon completion of the I-V test, one chip was mounted in a coplanar waveguide fixture. Prior to mounting the chip, the chip ground plane metal was removed along with approximately 1 mm of the coplanar waveguide center conductor. The chip was epoxied and wire bonded into the fixture as shown in Figure 10.

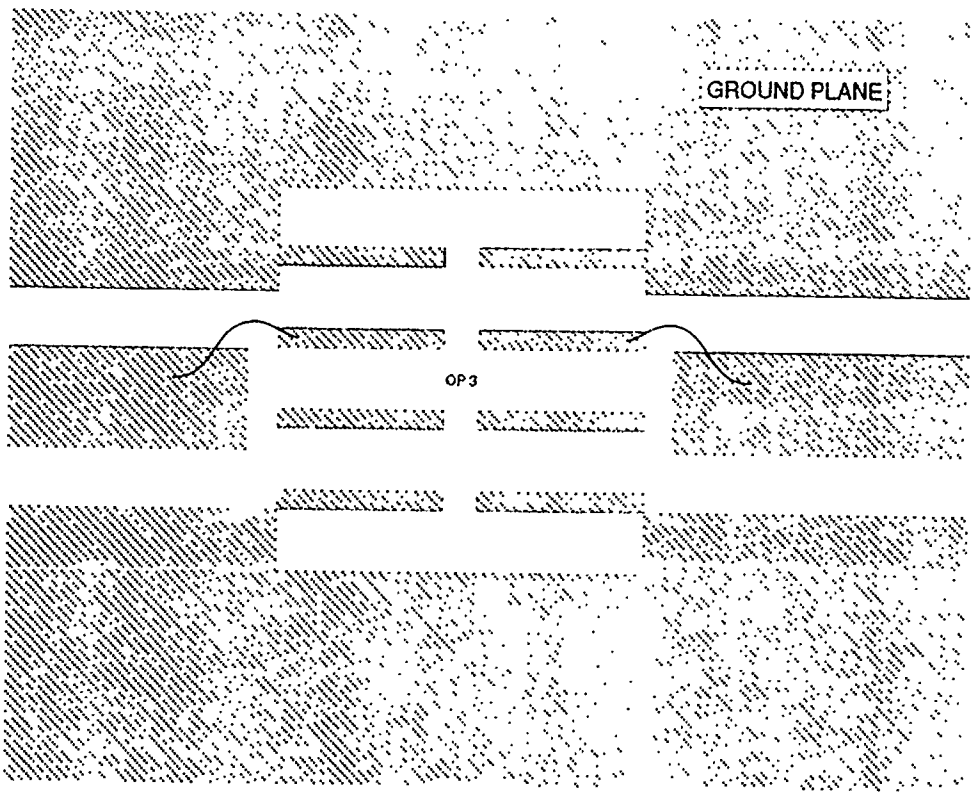

Figure 10. Switch Chip in Coplanar Waveguide Fixture.

Removal of the chip ground plane eliminates the microstrip structure of the chip and increases the impedance discontinuity, however, the chip is still small compared to the coplanar waveguide wavelength for frequencies up to several gigahertz and therefore may be considered a lumped element.

Using the setup shown in Figure 11, the switch characteristics were tested. The laser used in the experiment was a Nd:YLF solid state laser, with a nominal average power of 10 watts. The laser is capable of producing 35 picosecond (ps) pulses at a wavelength of 1.054 μm. When mode locked (ML), the pulse repetition frequency (PRF) is 76 MHz with a peak power of about 2 kilowatts. When the laser is both mode locked and Q-switched (QS), it is expected to produce a group of Q-switched 60 ps pulses each with a peak power of 1.2 megawatts at a 1 kHz PRF.

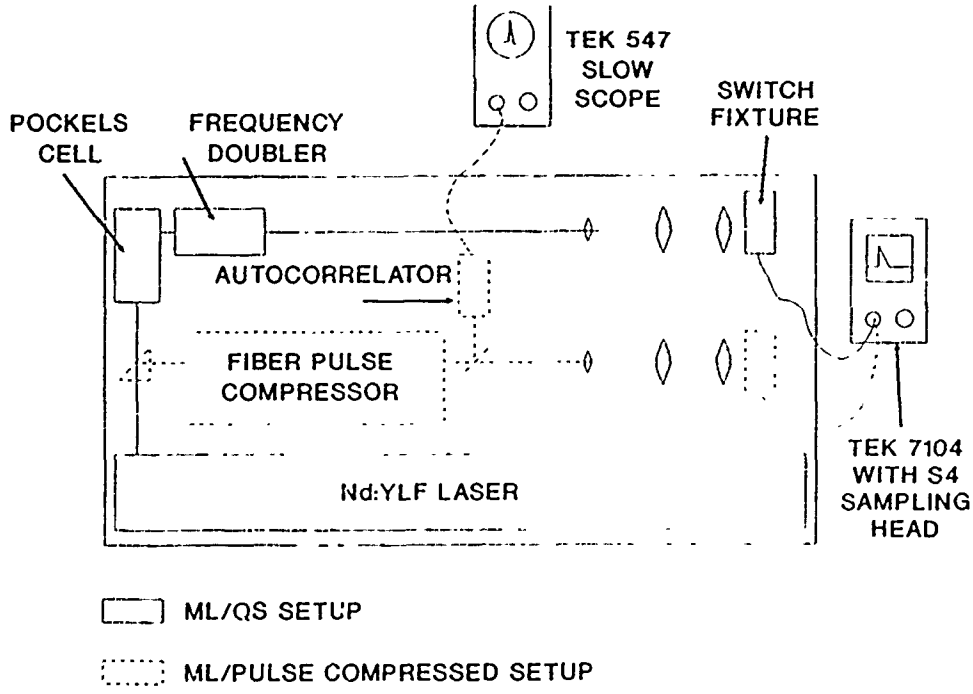

Figure 11. Experimental Setup.

Since 1.054 μm light (near infrared with energy of 1.18 eV) is below the band gap or absorption edge of semi-insulating GaAs [1.46 eV], the mode-lock/Q-switch output of the laser is frequency doubled. This is done using a Pockels cell to gate out one of the largest mode-lock/Q-switch pulse of the Q-switch group into a potassium titanyl phosphate (KTP) crystal.

The output power of a single green pulse should be about 750 kW peak and have a 60 ps width. However, subsequent measurements shown below indicate the Q-switch pulse to be much longer than 60 ps. In fact, the response of the experimental photoconductive switches and the response of a fast photodiode detector having a rise time of 35 ps, and put in place of the switch, show the same characteristic output as a function of time. The observed waveforms shown in Figure 12a are similar to the shape of the Pockels cell gate used to select a mode-locked pulse from the Q-switch group and shown in Figure 12b. The conclusion is that during Q-switch operation the laser, as presently operating, does not mode lock. We interpret our result as the Pockels cell selecting an approximately 10 nanosecond portion of the non-mode-locked Q-switch laser output. This pulse is doubled and focused onto the gap-switch. When first observed, this pulse shape caused much confusion until it was realized that the laser was not mode locked during Q-switch operation. There is no inherent problem that prevents mode-locked/Q-switch operation and laser upgrading and tuning procedures are being pursued to allow stable mode-locked/Q-switch operation in the near future.

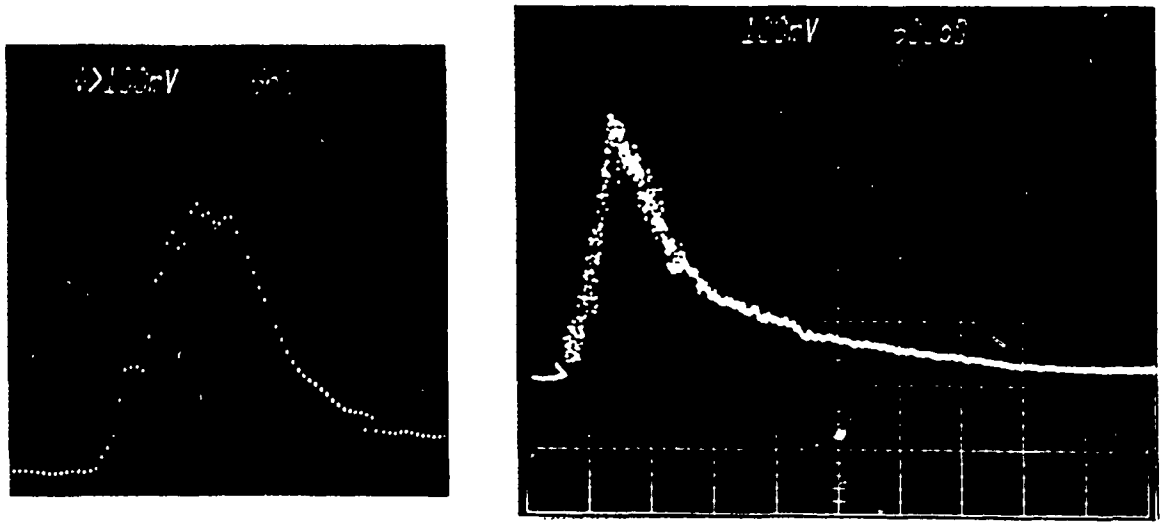

Figure 12. Comparison Traces of Photoconductive Switch Output (a), and Output of Pockels Cell Switching Out a Portion of Non-Mode-Locked Q-Switched Pulse (b).

Because of our inability to obtain high power picosecond pulses by Q-switch operation, present investigation of the experimental fast transient behavior of the gap switch was done using mode-locked/fiber-compressed pulses in the 3 ps range. Although an accurate picture of the gap photoconductive transient behavior is obtained using these techniques, there is not sufficient pulse energy, without Q-switching, to effectively close the switch in a 50 ohm impedance circuit. In other words, the switch resistance cannot be made much less than 50 ohms.

A spectra Physics Model 3690 fiber optic pulse compressor and frequency doubler is used to compress the Nd:YLF laser's approximately 35 ps mode-locked pulse to about 3 ps which is doubled to green 527 μm light. The green peak pulse power is estimated to be about 175 W at a pulse repetition frequency of 76 MHz.

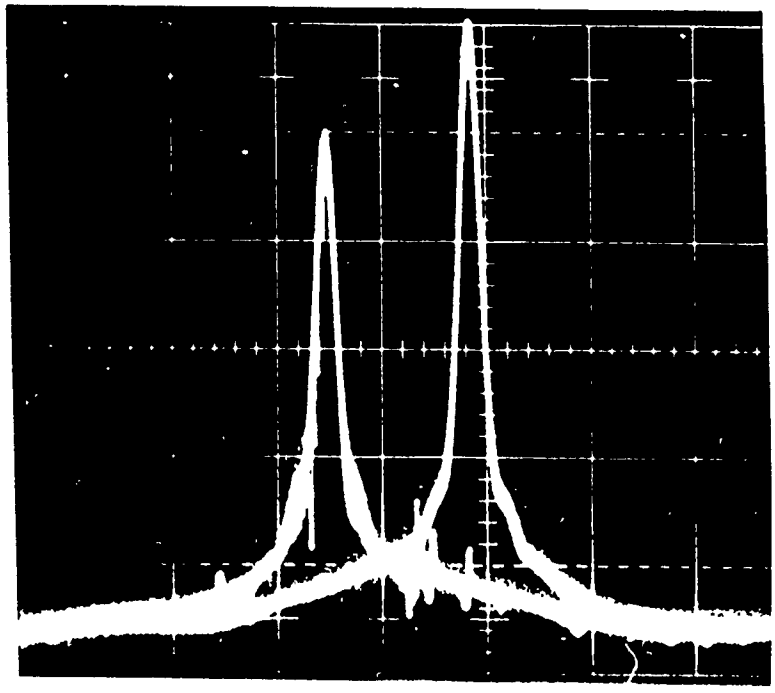

Figure 13. Pair of Autocorrelation Traces at 1.05 μm. Traces are displaced with 20 ps delay for scale calibration (≈15 ps/cm). Trace verifies approximately 4 ps pulsewidth of fiber/grating compressor.

Measurement of these short pulse widths is done using the 1.054 μm output from the compressor's doubler dump port, which goes into a modified Spectra Physics Model 409 autocorrelator. The dump port IR signal contains a significant (≈1 percent) amount of copropagating green light that must be blocked with a spatial filter (pin hole) inside the autotcorrelator, after the mixing crystal. The compressed IR autocorrelation trace actually measured, shown in Figure 13, is seen to be consistent with an ≈4 ps pulse. The doubled green pulse would be less than this or about 3 ps. The 0.527 μm light from the doubler is expanded and focused to a round spot which slightly overfills the gap switch mounted in a 50 ohm microstrip fixture. The peak light intensity on the gap is estimated to be about 2MW/cm^2, well below the damage threshold (>10^{9}W/cm^2) for GaAs.

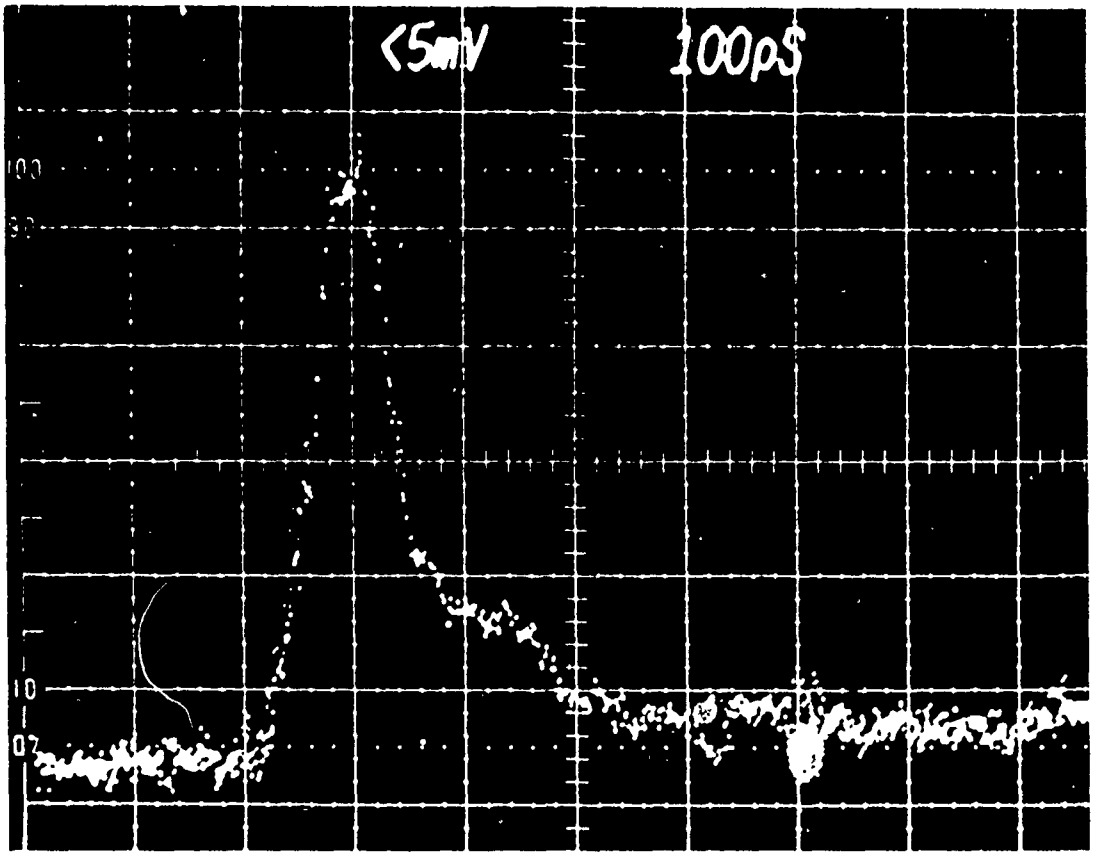

Figure 14. Pulse Response of GaAs Gap Switch to 3 ps, 0527 μm Pulse.

The response of a typical gap-switch to 3 ps green pulses, measured by an Opto-Electronics PD-15 wideband photodiode and displayed on a Tektronix 7104/7S11/S4 sampling oscilloscope is shown in Figure 14. Similar response is shown by both ohmic and non-ohmic contact devices. Modeling of switch material properties needed to produce this response is given in detail below. However, it is clear that although the switch closes quickly, it does not stay closed long enough to pass even a fraction of a cycle of a 6 GHz waveform (period = 166 ps). In fact, the actual switch response is shorter than shown because the displayed pulse is bandwidth limited by the pulse measuring system, that is, cables and oscilloscope sampling head.

3.5 Modeling and Analysis of PC Switches

As a precursor to modeling the entire frozen wave generator on SPICE, the resistance of the switch, as a function of time, was modeled with the mathematics software package MATHCAD. Using the measured average power and pulse width, we estimated the peak power and energy

per pulse. The equations given in Section 3.3 [Eqs. (16)-(25)] were then used to generate the carrier concentration. Combining the carrier concentration and mobilities, we calculated the conductivity.

Finally, inserting the light penetration depth and switch geometry, we calculated the resistance with Eq. (26). This resistance was placed in the simple circuit shown in Figure 15. At present, we are neglecting the parasitic capacitances C_g, and junction effects of the full blown Ebers-Moll model of Figure 8. This is a preliminary attempt at fitting data to an oversimplified model. In the future when better switch performance is expected through the use of longer carrier lifetime material the switch will be modeled using SPICE. This will include the junction effect and parasitic capacitance C_g.

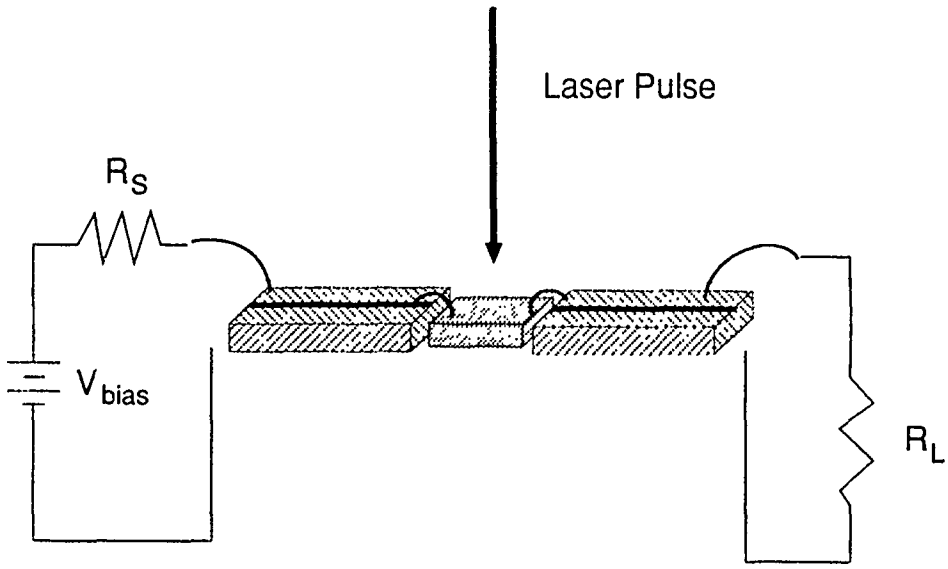

Figure 15. Simplified Switch Network.

The voltage at the load is given by

$$V_L = \frac{V_{bias}}{2} \cdot \frac{R_l}{R_l + R(t)} \quad (26)$$

The output of the simulation with the following parameters is shown in Figure 16.

Average Power = 35 mW

Pulse Width = 3 ps
Mobilities: $\mu_n = 8500\ cm^2/V \bullet s$, $\mu_p = 400\ cm^2/V \bullet s$
Gap Length = 75 μm
Gap Width = 68 μm
Gap Depth = 0.2 μm

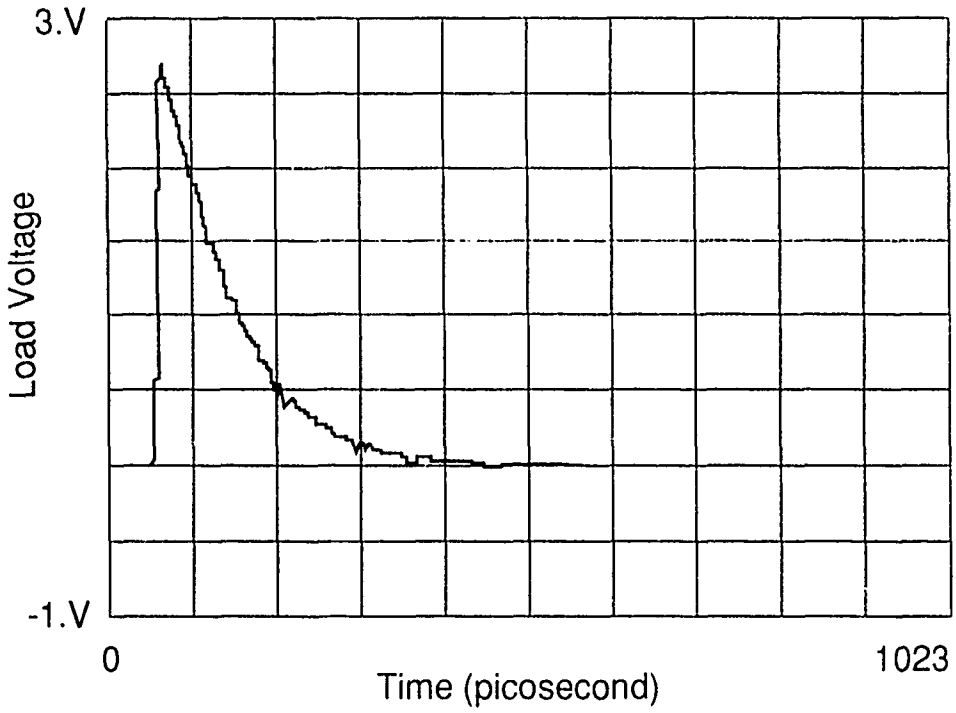

Figure 16. Simulated Output Voltage.

3.6 Comparison of Model to Experimental Results

Comparing the simulation with the experimental results given in Section 3.4, we see that the model rise time is shorter and the carrier lifetime is on the order of 50 ps. The slower experimental rise time can be attributed to parasitic capacitances not included in the model and the rise time (~100 ps) of the oscilloscope. The fall time of the switch is much shorter than desired. The short lifetimes can be attributed to the device's processing. The details of the processing are sketchy. To our knowledge, the wafer was processed using ion implantation. The region in the gap was then etched to expose the semi-insulating GaAs. From the lifetimes seen experimentally, it would appear that not enough of the doping "tail" of

the n+ layer was removed. Although the wafer was annealed, we believe the semi-insulating substrate contained enough damage and impurities to reduce the lifetime to 50 ps.

4.0 SUMMARY

We have shown how FWG performance depends on material characteristics of both the energy storage lines and photoconductive switch. Preliminary photoconductive switches of various gap geometries made in semi-insulating GaAs were built and tested in a broad band microwave test fixture excited by 3 ps pulses from a mode-locked, pulsed-compressed, frequency-doubled Nd:YLF laser. Analysis of the switch photoresponse yields a measured carrier lifetime of approximately 50 ps. This lifetime is too short for a practical FWG. The extension of this work, to find and use longer lifetime switch material, is directed to intrinsic silicon on sapphire, InP and high purity GaAs. Work is in progress to investigate these materials using the above techniques and then incorporate the appropriate material in a C-band FWG.

References

1. Haykin, Simon (1983) *Communication Systems, 2nd Ed.*, New York, NY, John Wiley and Sons, p. 29.

2. Proud, J.M. and Norman, S.L. (1978) High frequency waveform generation using optoelectronic switching in silicon, *IEEE Trans. Microwave Theory Tech.*, **MTT-26**:137.

3. Lee, C.H., Li, M.G., Chang, C.S., Yurek, A.M., Rhee, M.J., Chauchard, E., Fischer, R.P., Rosen, A., and Davis, H. (1985) Optoelectronic techniques for microwave and millimeter-wave applications, *Proc. IEEE-MTT-S International Microwave Symposium*, St. Louis, MO, p. 178.

4. Gupta, K.C., Garg, R., and Bahl, I.J. (1979) *Microstrip Lines and Slotlines*, Dedham, MA Artech House, p. 88.

5. Bahl, I.J. and Bhartia, P. (1980) *Microstrip Antennas*, Dedham, MA, Artech House, p. 309.

6. SUPERCOMPACT, for example, is one such software package.

8. Auston, D.H. Chapter 4 in Lee, C.H., ed., (1984) *Picosecond Optoelectric Devices*, New York, NY, Academic Press.

9. Maeda, M. (1972) An analysis of gap in microstrip transmission lines, *IEE Trans. Microwave Theory Tech.*, **MTT-20**:390.

10. Muller, R.S. and Kammis, T.I. (1981) *Device Electronics for Integrated Circuits, 2nd Ed.*, New York, NY, John Wiley and Sons, p. 294.

11. Sze, S.M. (1981) *Physics of Semiconductor Devices, 2nd Ed.*, New York, NY, John Wiley and Sons, p. 745.

12. Nunnaly, W.C. and Hammond, R.B. (1984) Chapter 12, in Lee, C.H., ed., *Picosecond Optoelectric Devices*, New York, NY Academic Press.

13. Lee, C.H. (1984) Chapter 5 in Lee, C.H., ed., *Picosecond Optoelectric Devices*, New York, NY, Academic Press.

14. Bube, R.H. (1960) *Photoconductivity of Solids*, New York, NY, John Wiley and Sons, p. 78.

Appendix A

Acronyms

CPW	coplanar waveguide
FWG	frozen wave generator
GaAs	gallium arsenide
IR	infrared
I–V	current-voltage
KTP	potassium titanyl phosphate
ML	mode locked
MS	microstrip
Nd:YLF	neodymium doped yttrium lithium fluoride
PC	photoconductive
PRF	pulse repetition frequency
ps	picosecond
QS	Q-switched
RF	radio frequency
SI	semi-insulating

Appendix B

Definition of Variables

A	amplitude of pulse
C_g	gap capacitance
d	effective absorption depth
e	electron charge
E_g	energy band gap of semiconductor
f	frequency
f_o	center frequency
Δf	frequency spread about f_o
h	semiconductor substrate thickness
$h\upsilon$	photon energy
I_B	optically injected "base" current
N	number of cycles in frozen wave
Δn (t)	optically induced carrier concentration change
P	width (temporal) of the microwave pulse (= TN)
P (t)	optical power
R	switch resistance
r	reflectivity of semiconductor
t	microstrip thickness
t_t	transit time

T	period of microwave pulse
V_p	phase velocity
w	microstrip width
X	line length between switches
Z_o	transmission line characteristics impedance
α_c	strip conductor attenuation constant
α_d	dielectric attenuation constant
β	absorption
Γ	reflectivity of semiconductor
γ	time constant
ε_r	static relative dielectric constant
ε_{re}	effective relative dielectric constant
η	quantum efficiency
μ_n	electron mobility
μ_p	hole mobility
σ_c	conductivity of strip conductor
σ_d	conductivity of semiconductor
τ	carrier lifetime